Scottish Universities Environmental Research Centre

Luminescence Measurements of a Monolith Sample From Twmbarlwm, Caerphilly.

October 2023

A.J. Cresswell[1], D.C.W. Sanderson[1], R. Hankinson[2], T. Malim[2]

[1]SUERC, East Kilbride, Glasgow
[2]Clwyd and Powys Archaeological Trust

East Kilbride Glasgow G75 0QF Telephone: 01355 223332 Fax: 01355 229898

Summary

Twmbarlwm is a univallate enclosure with a substantial mound, occupying a dominant position at the highest point and south-western terminus of the Mynydd Maen ridge to the north of Risca, Caerphilly. The site is conventionally understood as an Iron Age hillfort modified with a medieval motte, though it has also been suggested that the motte and enclosure are contemporary, and conversely that the site originated as a Neolithic causeway enclosure. During excavations of the bank and ditch at a terminus adjoining an apparent gap in the enclosure a 50cm long monolith sample was collected through the rampart, including the top soil and a context interpreted as top soil at time of construction of the rampart. This was sent to SUERC for luminescence analysis.

After removing potentially light exposed surfaces, 12 pairs of small samples were taken down the length of the monolith, which were used for portable OSL and laboratory profile measurements. Portable OSL measurements showed only small variations in OSL and IRSL counts and depletion indices for the top of the profile, with the bottom 1 or 2 samples showing reduced counts and in increase in OSL depletion. The laboratory measurements showed small variations in sensitivity without any clear trends, and OSL apparent doses for all samples consistent with archaeological ages. The TL apparent doses showed three zones corresponding to the observed differences in the monolith soils, with higher doses (>200Gy) in the upper 25cm of dark sediment, doses of 50-200Gy in the orange silt interpreted as bank deposits, and <50Gy in the bottom sample of compacted sediment interpreted as the pre-construction ground surface. These data are consistent with the interpretation of the compacted sediment as the old ground surface which had been light exposed prior to the construction of the bank, though further samples from below this would have been needed to confirm this.

Three samples were taken from the monolith for dating, with potentially light exposed surfaces removed first and dried for dose rate determination. These were taken from the top of the orange silt (SUTL3190/8 at 30cm), the bottom of the orange silt (SUTL3190/11 at 44cm) and the compacted sediment (SUTL3190/12 at 48cm). SUTL3190/12 gives a date of 20 ± 120AD, which assuming this is the old ground surface would a TPQ for the construction of the bank. SUTL3190/11 gives two main dates of 15 ± 120AD and 1340 ± 250BC suggesting a mixture of material with some the same date as the consolidated sediment below and some 1000-1500 years older. The combination of the younger dates for these two samples gives a revised date of **20 ± 85AD**. SUTL3190/8 gives a low precision date of 530 ± 250BC.

The date is consistent with construction of the earthworks at this location in the late Iron Age or early Roman period and is inconsistent with suggestions that this part of the enclosure is associated with the medieval motte or a preceding Neolithic enclosure.

Contents

List of figures

List of tables

1. Introduction

Twmbarlwm is a prominent hill and scheduled monument to the north of Risca, Caerphilly County, which occupies a dominant position at the south-western terminus and highest point of the Mynydd Maen ridge. The monument comprises a univallate enclosure occupying approximately 4.14 ha, conventionally understood as an Iron Age hillfort, and a substantial mound, interpreted as a medieval motte. It has been suggested that the enclosure and motte could be contemporary. It has also been suggested that the monument could have originated as a Neolithic causewayed enclosure, based on radiocarbon dating and some sections of the earthworks.

A series of geophysical surveys was conducted under the direction of Clwyd-Powys Archaeological Trust (CPAT) following fires in 2018 that cleared away surface vegetation, with UAV photogrammetry with accompanying ground-truthing and paleoenvironmental investigations. Excavations by CPAT and volunteers from the Cymdeithas Tymbarlwm Society were conducted in August 2021, with two test pits to investigate geophysical anomalies and three trenches investigating a bank and ditch terminal adjoining an apparent gap in the enclosure rampart (Trench 1); a sub-circular feature seen on the interior face of the enclosure bank (Trench 2); and the corresponding section of the enclosure ditch (Trench 3). The trench locations are shown in Fig. 1.1. The results of these investigations are reported in Hankinson (2022).

During the excavation of Trench 1, a 50cm long monolith sample was extracted from the northern part of the trench, through the rampart including the top soil and subsoil. The location of this shown in Fig. 1.2, with a photograph of this face of trench 1 in Fig. 1.3. This sample was carefully wrapped to maintain physical cohesion and prevent further light exposure, with the top and bottom ends clearly marked, and shipped to the Scottish Universities Environmental Research Centre (SUERC) for luminescence analysis. These analyses are reported here.

Contexts 1 and 2 in Fig. 1.2 extend across the entire area of Trench 1, and are interpreted as soils that have developed since completion of the monument. The ditch with its fill (context 7) appears to cut into context 8, and thus context 8 is interpreted as the natural subsoil whose upper surface is likely to have been exposed at the time the rampart was constructed in this location. Context 5 is, thus, interpreted as the material used to construct the rampart, presumably removed from the ditch.

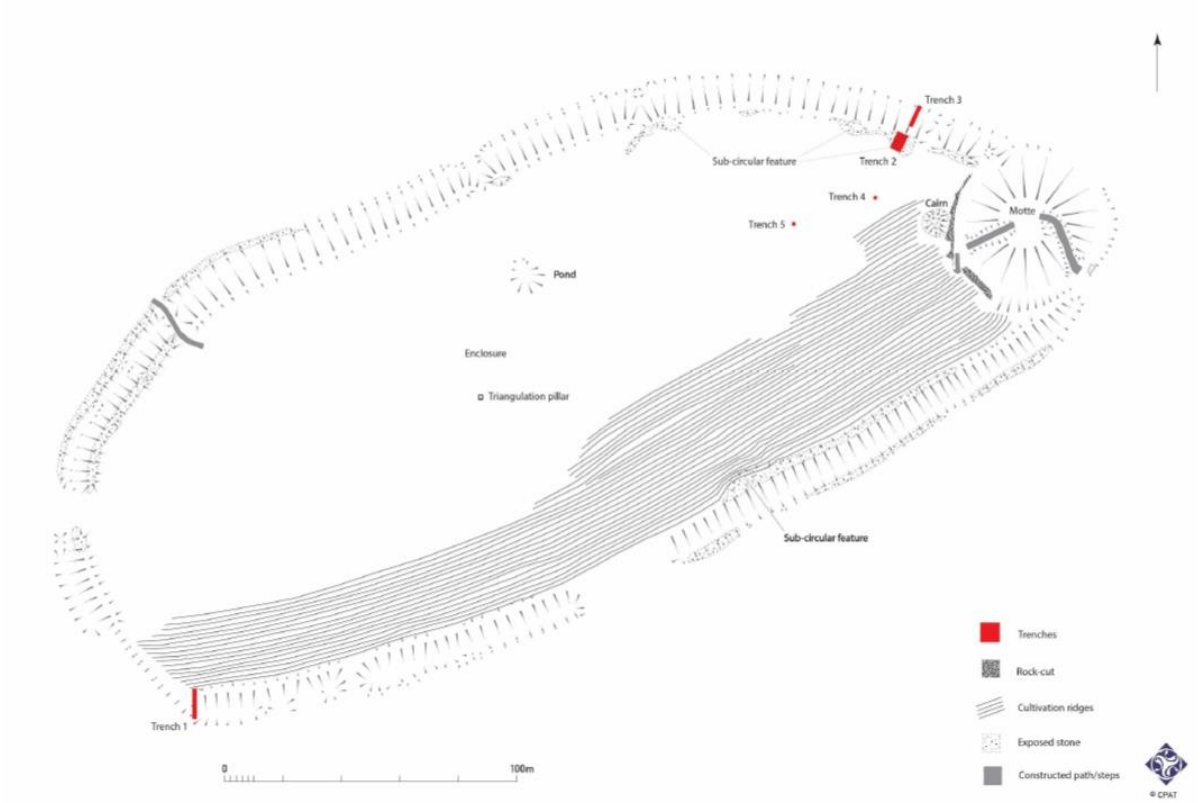

Figure 1.1: Plan of Twmbarlwm showing earthworks and excavation trenches. Taken from Hankinson (2022).

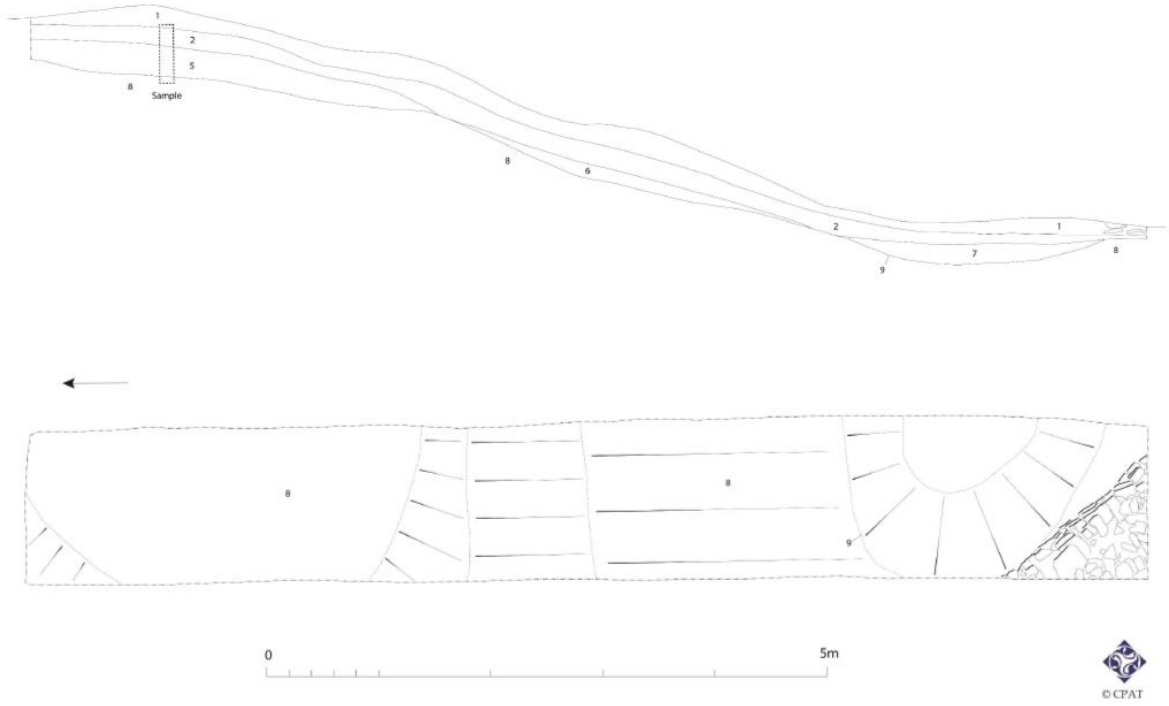

Figure 1.2: Plan and section of trench 1, showing the location of the monolith sample. Taken from Hankinson (2022).

Figure 1.3: Photograph of section through the enclosure bank, looking east. The monolith sample (not shown) was collected through the northern part of the section, just to the left of the pole. Taken from Hankinson (2022).

2. Methods

2.1. Sampling and sample preparation

The sample was carefully opened at SUERC under safelight conditions. Differences in sediment texture down the section were noted, with four different layers observed which should correspond to the four contexts in Fig. 1.2. The outer face, already exposed to daylight, was photographed under white lights. Twelve sampling positions were identified, with spacing of about 4cm down the section, trying to ensure that at least two samples were located in each identified sedimentary context and samples were placed either side of interfaces. Light exposed surface material was removed at each sampling position, and two 15mm diameter 25mm long copper tubes inserted at approximately 10cm separation, giving duplicate samples for each location. The positions of each tube were recorded and photographed, before removal of the tubes under safe light conditions and emptying content into 50mm diameter petri dishes for portable OSL measurement. The samples are summarised in Table 2.1, with the photographs showing sampling positions in Fig. 2.1.

Table 2.1: Summary of samples and SUERC laboratory reference codes

SUERC code	Depth	Description
SUTL3190/1	4	Unconsolidated dark soil – considered to be top soil (1)
SUTL3190/2	7	Unconsolidated dark soil – considered to be top soil (1)
SUTL3190/3	10	Compressed dark sediment with stones – considered to be the brown silt (2)
SUTL3190/4	14	Compressed dark sediment with stones – considered to be the brown silt (2)
SUTL3190/5	17	Compressed dark sediment with stones – considered to be the brown silt (2)
SUTL3190/6	22	Compressed dark sediment with stones – considered to be the brown silt (2)
SUTL3190/7	26	Compressed dark sediment with stones – considered to be the brown silt (2)
SUTL3190/8	30	Light coloured sediment with stones – considered to be the orange silt (5)
SUTL3190/9	34	Light coloured sediment with stones – considered to be the orange silt (5)
SUTL3190/10	38	Light coloured sediment with stones – considered to be the orange silt (5)
SUTL3190/11	44	Light coloured sediment with stones – considered to be the orange silt (5)
SUTL3190/12	48	Compacted light coloured sediment – considered to be subsoil (8)

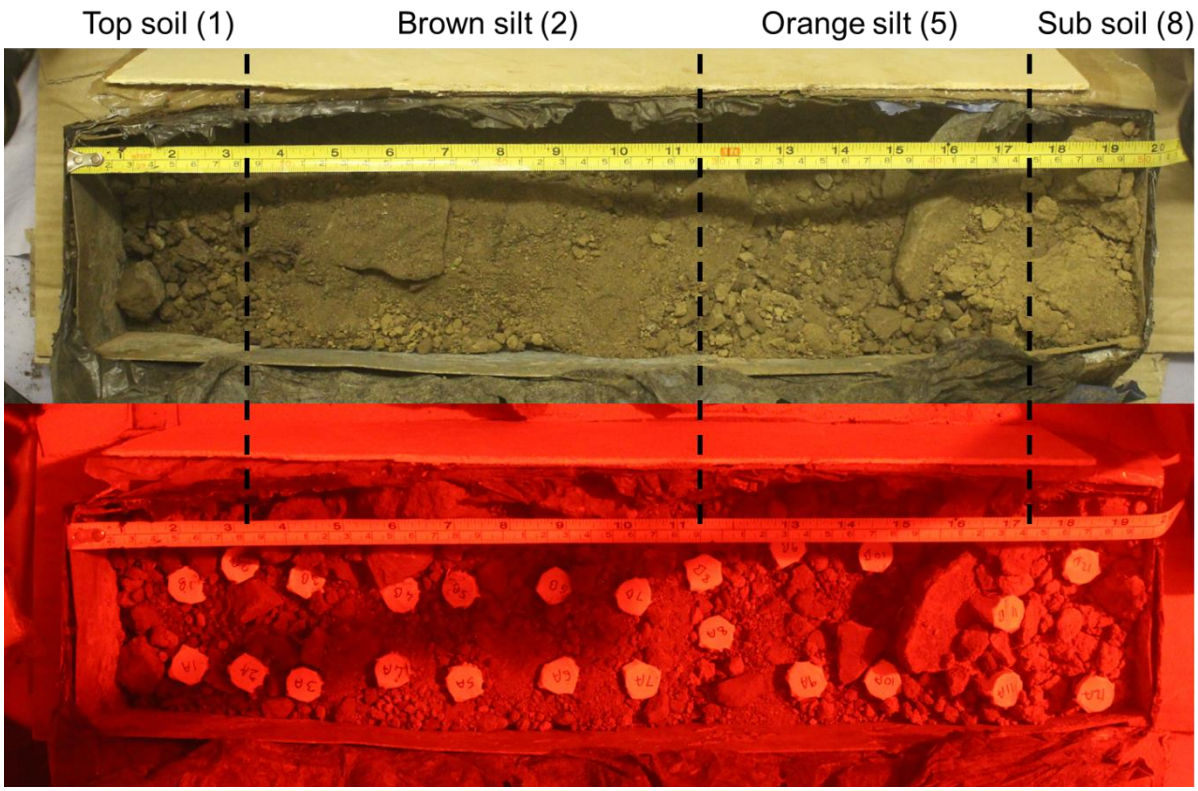

Figure 2.1: Photographs showing the monolith prior to removing light exposed surface with the identified stratigraphy indicated (top) and the sampling positions after removal of light exposed surface (bottom). The top of the monolith is to the left.

2.2. Portable OSL Measurements

The two 50mm diameter petri dishes for each position were appraised using the SUERC portable OSL reader, following an interleaved sequence of system dark count (background), infra-red stimulated luminescence (IRSL) and OSL, similar to that described by Sanderson and Murphy (2010). This method allows for the calculation of IRSL and OSL net signal intensities, depletion indices and IRSL:OSL ratios, which are then used to generate luminescence-depth profiles. These measurements allow a characterisation of the sediment sequences and an assessment of their potential for luminescence dating. Intensities are given as the net counts in 60s, after subtraction of the dark count background. The depletion index, evaluated as the ratio of the signal obtained in the first half of the stimulation period divided by that from the second half, is sensitive to the extent to which samples have been bleached prior to deposition, and IRSL:OSL ratios can vary in response to mineralogy.

2.3. Laboratory Profile Measurements

The portable OSL measurements would result in a small depletion of luminescence signals from grains at the surface, however the vast majority of grains are present in clumps and would be protected from signal depletion. Therefore, laboratory profile measurements of the materials used for portable OSL measurement would present a very small difference in signal intensity, without any loss of information on sensitivity or relative intensities down the section. The material from the "A" profile samples were wet sieved to extract the 90-250 µm grain size fraction. This was subjected to an acid treatment of 1M HCl for 10 minutes, 15% HF for 10 mins and 1M HCl for 10 mins, with the sample washed thoroughly with deionised water between each treatment. Approximately half of the material was retained, washed in acetone to displace water and dried as a polymineral sample. The remaining material was subjected to a further acid treatment of 40% HF for 40 mins and 1M HCl for 10 mins, with the sample washed thoroughly with deionised water between each treatment. This fraction was washed in acetone to displace water and dried as a nominal quartz sample.

Clean 10 mm diameter stainless steel discs were prepared with one side sprayed with silicone grease as an adhesive layer, with sample material dispensed as a monolayer onto the central ~5 mm of the disc. For each sample, a pair of polymineral and a pair of quartz discs were dispensed. All sample handling and preparation was conducted under safelight conditions in the SUERC luminescence dating laboratories.

Luminescence sensitivities (Photon Counts per Gy), sensitivity changes and stored doses (Gy) were evaluated from the paired aliquots of the polymineral and HF-etched quartz fractions, using Risø DA-15/DA-20 automatic readers equipped with a $^{90}Sr/^{90}Y$ β-source for irradiation, using blue LEDs emitting around 470 nm (OSL) and infrared (laser) diodes emitting around 830 nm (IRSL) for optical stimulation, and a U340 detection filter pack to detect in the region 270-380 nm. For quartz, each measurement was preceded by a pre-heat at 200°C for 10s, with a 30s OSL measurement at 125°C. Measurements were conducted for the natural signal, and following nominal 5 Gy and 50 Gy irradiations, with all measurements accompanied by a nominal 1 Gy test dose. For the polymineral samples, each measurement was preceded by a pre-heat at 200°C for 10s, with a 30s IRSL measurement at 50°C and a TL measurement to 500°C. Measurements were conducted for the natural signal, and following nominal 5 Gy and 50 Gy irradiations. No test dose measurements were included.

2.4. Dose rate measurements

Three positions from the 12 sampled for profiling were selected as promising locations for OSL dating, along with two additional locations which could be of interest for additional dating if required. Additional potentially light exposed surface material was removed at each of these locations, before approximately 20g of material was removed as the dating sample. The potentially light exposed material, including that removed while collecting the profile samples, was used for dose rate measurements.

This material was lightly ground to break up clumps of sediment without cracking the stones present, and 20g of the fine material removed for Thick Source Beta Counting (TSBC) using the SUERC TSBC system (Sanderson, 1988). Count rates were determined with six replicate 600s counts on each sample, bracketed by background measurements and sensitivity determinations using the Shap Granite secondary reference material. Infinite-matrix dose rates were calculated by scaling the net count rates of samples and reference material to the working beta dose rate of the Shap Granite (6.25 ± 0.03 mGy a^{-1}). The estimated errors combine counting statistics, observed variance and the uncertainty on the reference value.

The remaining material was ground to break up stones into sand sized grains or smaller, with the material for TSBC mixed in after the beta dose rates had been measured. Approximately 50g of this material was dispensed into 50mm diameter x 40mm polypropylene containers for High Resolution Gamma Spectrometry (HRGS) measurements using a 50% relative efficiency "n" type hyper-pure Ge detector (EG&G Ortec Gamma-X) operated in a low background lead shield with a copper liner. Gamma ray spectra were recorded over the 30 keV to 3 MeV range from each sample, interleaved with background measurements and measurements from SUERC Shap Granite standard in the same geometries. Sample counts were 80 ks. The spectra were analysed to determine count rates from the major line emissions from ^{40}K (1461 keV), and from selected nuclides in the U decay series (^{234}Th, ^{226}Ra + ^{235}U, ^{214}Pb, ^{214}Bi and ^{210}Pb) and the Th decay series (^{228}Ac, ^{212}Pb, ^{208}Tl) and their statistical counting uncertainties. Net rates and activity concentrations for each of these nuclides were determined relative to Shap Granite by weighted combination of the individual lines for each nuclide. The internal consistency of nuclide specific estimates for U and Th decay series nuclides was assessed relative to measurement precision, and weighted combinations used to estimate mean activity concentrations (Bq kg^{-1}) and elemental concentrations (% K and ppm U, Th) for the parent activity. These data were used to determine infinite matrix dose rates for alpha, beta and gamma radiation.

The dose rate measurements were used in combination with assumed burial water contents, to determine the overall effective dose rates for age estimation. Cosmic dose rates were evaluated by combining latitude and altitude specific dose rates 0.185 ± 0.010 mGy a^{-1} using the method of Prescott and Hutton (1994).

2.5. Quartz SAR measurements

Approximately 50 g of material was removed for each tube and processed to obtain sand-sized quartz grains for luminescence measurements. Each sample was wet sieved to obtain the 90-150 and 150-250 μm fractions. The 90-150 μm fractions were treated with 1 M hydrochloric acid (HCl) for 10 minutes, 15% hydrofluoric acid (HF) for 15 minutes, and 1 M HCl for a further 10 minutes. The HF-etched sub-samples were then centrifuged in sodium polytungstate solutions of 2.62, and 2.74 g cm^{-3}, to obtain concentrates of feldspars (<2.62 g cm^{-3}) and quartz plus plagioclase (2.62-2.74 g cm^{-3}). The selected quartz fraction was then subjected to further HF and HCl washes (40% HF for 40 mins, followed by 1M HCl for 10 mins).

All materials were dried at 50°C and transferred to Eppendorf tubes. The 40% HF-etched, 2.62-2.74 g cm^{-3} 'quartz' 90-150 μm fractions were dispensed to 10 mm stainless steel discs for measurement. Initially, 32 aliquots were dispensed for each sample.

Equivalent dose determinations were made on sets of 32 aliquots per sample, using a single aliquot regeneration (SAR) sequence (cf Murray and Wintle, 2000). Using this procedure, the OSL signal levels from each individual disc were calibrated to provide an absorbed dose estimate (the equivalent dose) using an interpolated dose-response curve, constructed by regenerating OSL signals by beta irradiation in the laboratory. Sensitivity changes which may occur as a result of readout, irradiation and preheating (to remove unstable radiation-induced signals) were monitored using small test doses after each regenerative dose. Each measurement was standardised to the test dose response determined immediately after its readout, to compensate for changes in sensitivity during the laboratory measurement sequence. The regenerative doses were chosen to encompass the likely value of the equivalent (natural) dose. A repeat dose point was included to check the ability of the SAR procedure to correct for laboratory-induced sensitivity changes (the 'recycling test'), a zero dose point is included late in the sequence to check for thermally induced charge transfer during the irradiation and preheating cycle (the 'zero cycle'), and an IR response check included to assess the magnitude of non-quartz signals. Regenerative dose response curves were constructed using doses of 1, 2, 3, 4, 8 and 12 Gy, with test doses of 1.0 Gy. The 32 aliquot sets were sub-divided into four subsets of eight aliquots, such that four preheating regimes were explored (200°C, 220°C, 240°C and 260°C). All measurements were conducted using a Risø DA-15 automatic reader equipped with a $^{90}Sr/^{90}Y$ β-source for irradiation, blue LEDs emitting around 470 nm and infrared (laser) diodes emitting around 830 nm for optical stimulation, and a U340 detection filter pack to detect in the region 270-380 nm, while cutting out stimulating light (Bøtter-Jensen et al., 2000).

The data were processed to determine quality parameters for the SAR procedure, with any aliquot which failed these tests rejected from further analysis, as follows.
1. The sensitivity (c Gy^{-1}) was determined from the response to the first test dose
2. The sensitivity change is determined from the difference between the last and first test dose responses divided by the number of measurement cycles, as a percentage of the first test dose.
3. The recycling ratio is the ratio of the normalised OSL measurement for the repeat of the first regenerative dose divided by the normalised OSL measurement for the first regenerative dose. This should be unity.
4. The zero cycle response is the normalised OSL measurement following the zero dose cycle. This should be zero.

5. The IR response is the ratio of the response to IR stimulation following a 1Gy dose to the response to blue stimulation following a 1Gy dose. This should be zero.
6. The dose recovery test uses the response to the first test dose normalised using the response to the first regenerative dose to confirm that the curve fitting returns the test dose value. This should be 1Gy.

For each regenerative dose, the OSL counts normalised using the corresponding test dose are plotted against dose and an exponential rise to maximum curve fitted through the data. These are plotted for the average of each of the four pre-heating groups and for all samples (the plots for all samples are shown in Appendix C), and any differences between the pre-heating groups noted. Any aliquots showing significantly different dose responses compared to the other aliquots are removed from the analysis. The equivalent dose for each aliquot is determined by interpolation of the normalised natural OSL counts to the fitted curve.

l

3. Results

3.1. Portable OSL Measurements

The portable OSL results are shown in Fig. 3.1, with the data tabulated in Appendix A. There is good reproducibility between the pairs of aliquots at each position. With the exception of the bottom two samples, there are only small differences down the section. The bottom sample (at 48cm) shows a significant reduction in OSL and IRSL net counts, an increase in OSL depletion index and a lower IRSL:OSL ratio. The sample above this (at 44cm) has a slightly lower OSL count and slightly higher OSL depletion compared to the samples above it.

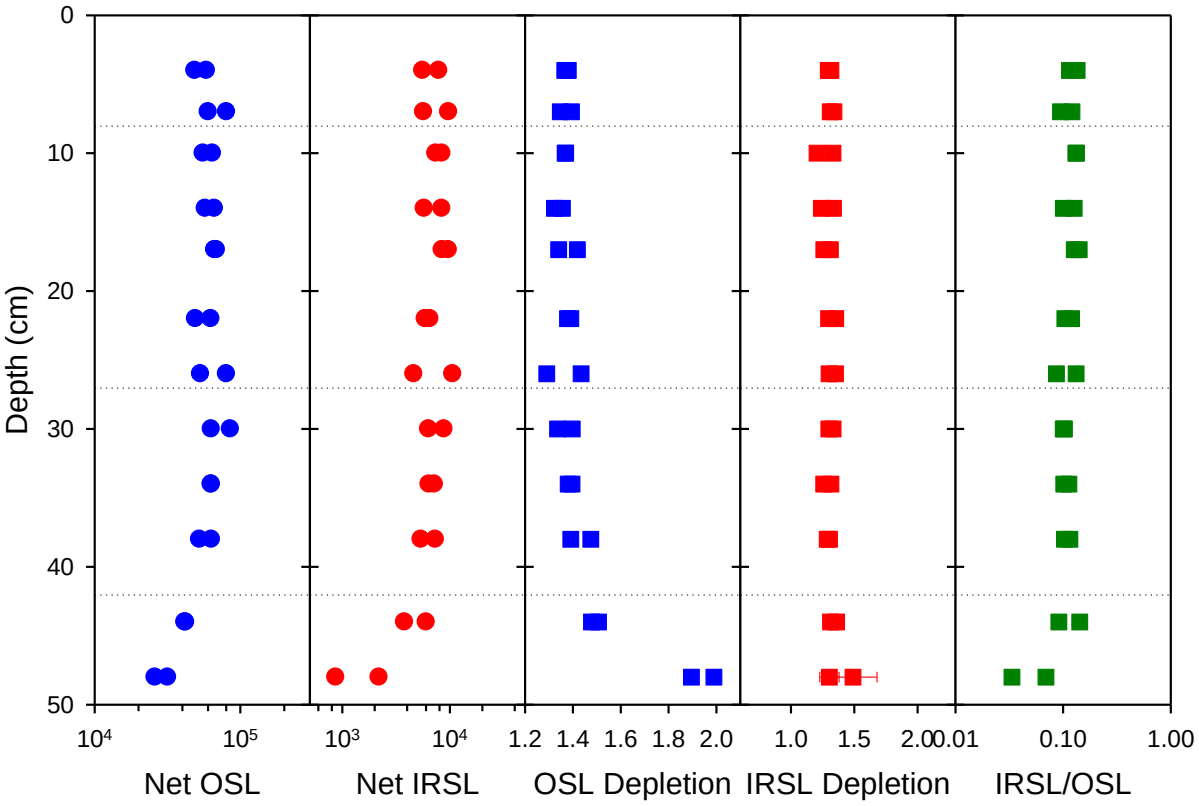

Figure 3.1: Portable OSL results showing net counts for OSL and IRSL, depletion indices for OSL and IRSL, and the ORSL:OSL ratio. The dotted horizontal lines indicate the approximate positions of the interfaces between the layers identified by visual inspection of the sample.

3.2. Laboratory Profile Measurements

The sensitivity and apparent dose determined from the OSL measurements of nominal quartz and the OSL, IRSL and TL measurements of polymineral aliquots are shown in Figs. 3.2 and 3.3, with the data tabulated in Appendix B.

The sensitivities (Fig. 3.2) are all generally low, less than 100 c Gy^{-1} for IRSL and less than 1000 c Gy^{-1} for OSL and TL, with the exception of the OSL measurement of one aliquot of quartz from SUTL3190/6 (22cm) which gives a sensitivity of 4400 ± 100 c Gy^{-1}. There's no significant variation in sensitivity with depth.

The apparent dose measurements (Fig. 3.3) show values mostly between 1 and 10Gy for the OSL from quartz, between 10 and 100Gy for the OSL from polymineral aliquots, and 50 to 1000Gy for the IRSL and TL measurements. The OSL shows little significant variation with depth for both quartz and polymineral aliquots though there is a slight reduction in apparent dose for the bottom sample in the quartz OSL, the IRSL shows values of 10-100Gy between 10-40cm depth with doses of 100-1000Gy at deeper and shallower depths. The TL shows a stepped pattern of values around 1000Gy above 30cm, about 100Gy below this and about 30Gy for the bottom sample.

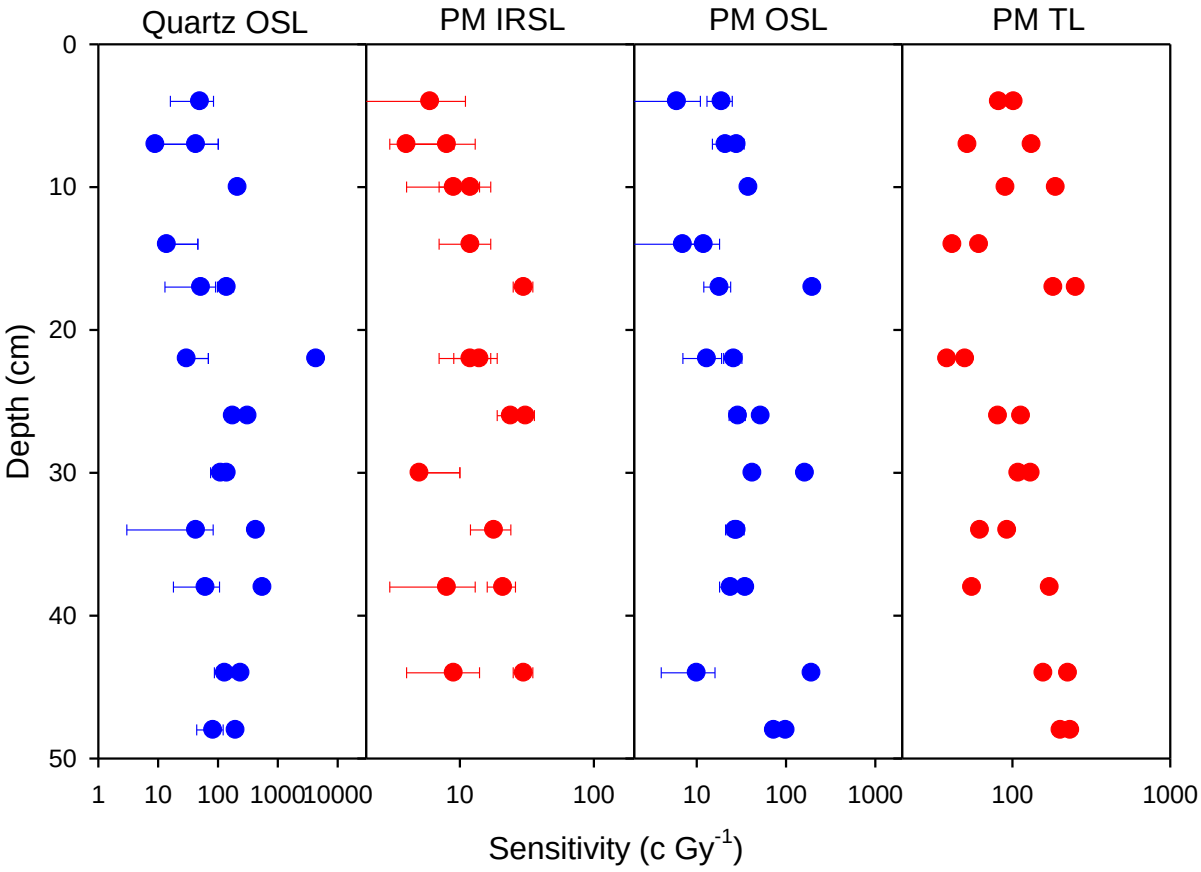

Figure 3.2: Sensitivities (c Gy^{-1}) measured using OSL from nominal quartz aliquots, and IRSL, OSL and TL from polymineral grains.

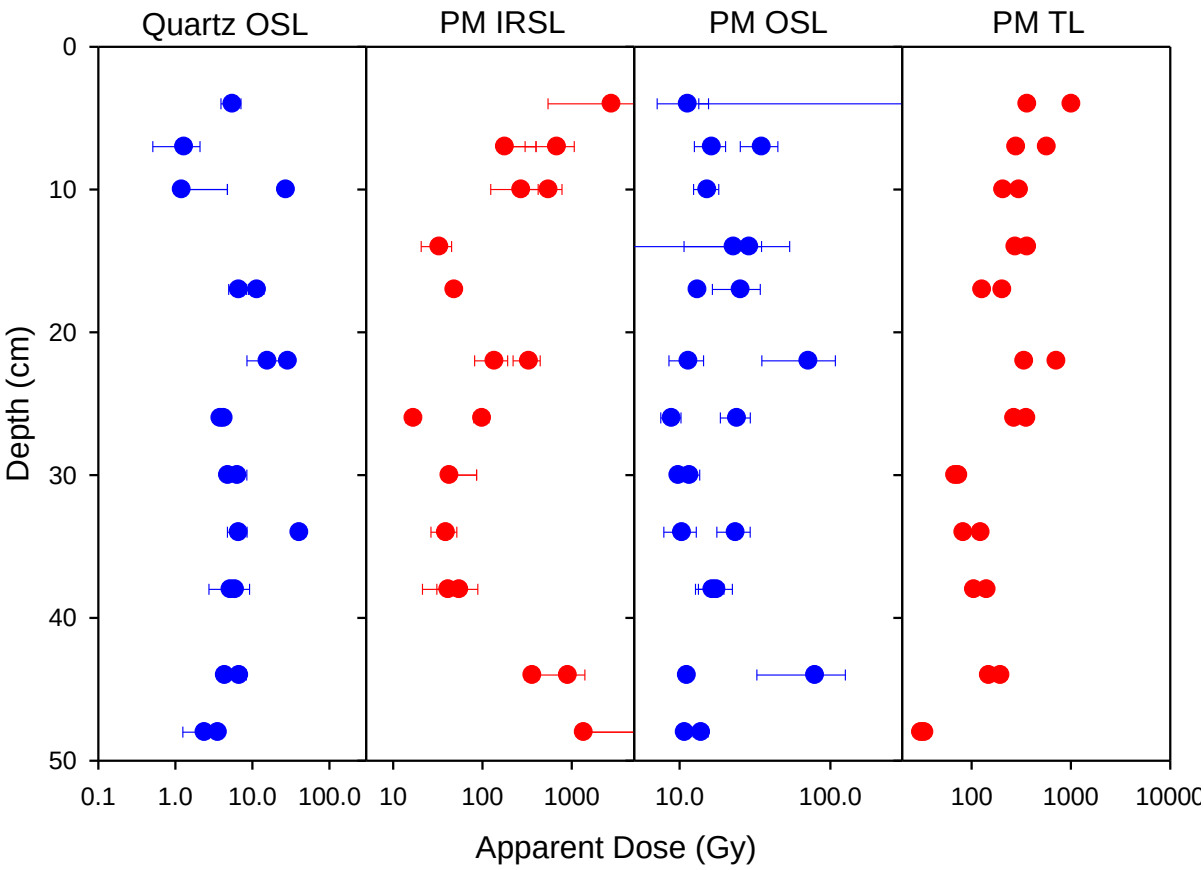

Figure 3.3: Apparent dose (Gy) measured using OSL from nominal quartz aliquots, and IRSL, OSL and TL from polymineral grains.

The laboratory profile data support the portable OSL profiles. With only small variations in sensitivity, the net OSL signals are explained by differences in apparent dose from the quartz OSL (with the reduced value for the bottom sample evident). The very low sensitivities for the IRSL and OSL from the polymineral aliquots suggests that feldspar signals would be too small to be useful. The pattern in the TL approximately matches the observations of sediment texture in the sample – with the highest apparent dose group corresponding to the darker sediments (contexts 1 and 2, interpreted as soils that have built up since construction of the monument), the group with apparent doses in the 60-200Gy range corresponding to the orange silt (context 5, interpreted and bank deposits), and the bottom sample at 30Gy corresponding to the compacted orange sediment (context 8, interpreted as the subsoil).

Based on the profiling data and stratigraphy, it was decided to take three samples for full dating at this time. SUTl3190/8 (30cm) is within context 5 (interpreted as bank deposit), and based on the TL and observation of the sample is at the top of this context although the section drawing suggests it's 5-10cm below the top of this context. SUTL3190/11 (44cm) is located on the interface between the bank (5) and the subsoil (8), potentially either the very bottom of the bank or top of subsoil. SUTL3190/12 (48cm) is within the subsoil (8) but carries the lowest OSL apparent dose and may represent the pre-construction landsurface.

3.3. Dose rate measurements

HRGS results are shown in Table 3.1, both as activity concentrations (i.e. disintegrations per second per kilogram) and as equivalent parent element concentrations (in % and ppm), based in the case of U and Th on combining nuclide specific data assuming decay series equilibrium.

Table 3.1: Activity and equivalent concentrations of K, U and Th determined by HRGS

SUTL no.	Activity Concentration[a] / Bq kg^{-1}			Equivalent Concentration[b]		
	K	U	Th	K / %	U / ppm	Th / ppm
3190/5	559 ± 28	26.4 ± 2.1	33.2 ± 1.9	1.81 ± 0.09	2.14 ± 0.17	8.17 ± 0.47
3190/7	549 ± 26	19.8 ± 2.2	27.3 ± 2.0	1.78 ± 0.09	1.60 ± 0.18	6.74 ± 0.48
3190/8	605 ± 26	21.6 ± 2.2	28.8 ± 1.9	1.96 ± 0.08	1.75 ± 0.18	7.11 ± 0.48
3190/11	478 ± 25	25.2 ± 2.2	28.4 ± 1.8	1.55 ± 0.08	2.04 ± 0.18	7.01 ± 0.45
3190/12	493 ± 23	24.8 ± 2.1	25.0 ± 1.9	1.59 ± 0.07	2.01 ± 0.17	6.17 ± 0.47

[a]Shap granite reference, working values determined by David Sanderson in 1986, based on HRGS relative to CANMET and NBL standards.

[b]Activity and equivalent concentrations for U, Th and K determined by HRGS (Conversion factors based on NEA (2000) decay constants): 40K: 309.3 Bq kg^{-1} %K^{-1}, 238U: 12.35 Bq kg^{-1} ppmU^{-1}, 232Th: 4.057 Bq kg^{-1} ppm Th^{-1}

Infinite matrix alpha, beta and gamma dose rates from HRGS are listed for all samples in Table 3.2, together with infinite matrix beta dose rates from TSBC. It can be seen that there is little variation in gamma dose rate between samples, and therefore the dose rates recorded for each sample can be used without the need to model gamma dose rates between samples in the absence of field gamma measurements. Also, the beta dose rate from HRGS, which includes stones, is consistently larger than the TSBC, which excludes stones, by 10-20%. This may reflect a slightly enhanced radionuclide concentration in the stones compared to the finer sediments. In calculating effective beta dose rates greater weight is given to the TSBC dose rates, since the beta dose rates experienced by mineral grains will be determined primarily by the finer sediments they're in rather than stones where the majority of beta radiation is absorbed by the stone.

Table 3.2: Infinite matrix dose rates determined by HRGS and TSBC

SUTL no.	HRGS, dry[a] / mGy a^{-1}			TSBC, dry / mGy a^{-1}
	Alpha	Beta	Gamma	
3190/5	12.00 ± 0.60	2.08 ± 0.08	1.09 ± 0.04	1.70 ± 0.07
3190/7	9.44 ± 0.61	1.93 ± 0.08	0.95 ± 0.04	1.72 ± 0.07
3190/8	10.12 ± 0.61	2.12 ± 0.08	1.03 ± 0.04	1.63 ± 0.08
3190/11	10.87 ± 0.60	1.81 ± 0.08	0.95 ± 0.04	1.44 ± 0.07
3190/12	10.16 ± 0.58	1.82 ± 0.07	0.92 ± 0.04	1.44 ± 0.08

[a]based on dose rate conversion factors in Aitken (1983), Sanderson (1987) and Cresswell et.al. (2018), and include uncertainties on conversion factors from Cresswell et.al. (2018).

The water content measurements are given in Table 3.3, together with the assumed values for the average water content during burial. Effective beta dose rates to the HF-etched 90-150 μm quartz grains are also given in table 3.3 (the mean of the TSBC and HRGS data, accounting for water content and grain size), together with the estimate of the gamma dose rate (HRGS data, accounting for water content). The total effective dose rate is the sum of these plus a cosmic contribution.

Table 3.3: Effective beta and gamma dose rates following water correction.

SUTL no.	Assumed water content / %	Effective Dose Rate / mGy a^{-1}		
		Beta[a]	Gamma	Total[b]
3190/5	20 ± 7	1.37 ± 0.10	0.82 ± 0.05	2.37 ± 0.11
3190/7	20 ± 7	1.34 ± 0.10	0.78 ± 0.06	2.31 ± 0.12
3190/8	20 ± 7	1.35 ± 0.10	0.84 ± 0.06	2.37 ± 0.12
3190/11	20 ± 7	1.17 ± 0.09	0.78 ± 0.06	2.13 ± 0.11
3190/12	20 ± 7	1.17 ± 0.09	0.75 ± 0.06	2.11 ± 0.11

[a] Effective beta dose rate combining water content corrections with inverse grain size attenuation factors obtained by weighting the 90-150 μm attenuation factors of Mejdahl (1979) for K, U, and Th by the relative beta dose contributions for each source determined by Gamma Spectrometry;
[b] includes a cosmic dose contribution

3.4. Quartz SAR measurements

The quality parameters for the aliquots with measurable test dose responses and that meet the other criteria for acceptability (recycling ratio consistent with unity, zero cycle consistent with zero and low IRSL) are given in Table 3.4. It can be seen that there's an increase in the number of accepted aliquots and the mean sensitivity of these, and a corresponding decrease in the uncertainties of the other parameters, for the lower samples.

Table 3.4: SAR quality parameters showing the number of selected aliquots, and for these the mean sensitivity, sensitivity change per cycle, the zero counts, recycling ratio, dose recovery and IRSL contribution.

SUTL No.	n	Sensitivity (c Gy^{-1})	Sensitivity change (%)	Zero	Recyling ratio	Dose recovery (Gy)	IRSL (%)
3190/8	7/32	376 ± 71	21.6 ± 11.9	0.06 ± 0.20	1.32 ± 0.29	1.14 ± 0.40	16.6 ± 3.7
3190/11	36/64	508 ± 69	13.2 ± 4.3	-0.04 ± 0.04	1.21 ± 0.10	0.99 ± 0.34	4.3 ± 1.2
3190/12	28/32	554 ± 48	14.4 ± 4.1	-0.11 ± 0.04	1.18 ± 0.12	0.77 ± 0.20	2.3 ± 0.9

Saturating exponential rise fits on the regenerative dose data resulted in large uncertainties on the parameters from the fits. As the dose regenerations follow linear relationships for the points at 8Gy and below, linear regression was used to produce equivalent dose values for each aliquot, this will result in a bias to lower dose values for aliquots with >8Gy doses, however as these would represent residual signals from older material this is not considered important to dating well zeroed minerals. Table 3.5 gives the equivalent dose calculated by different means from the distribution of doses for each aliquot – unweighted mean, mean weighted by uncertainty, a robust mean calculated using the AMC (2001) algorithm, and modelled minimum age (Galbraith et.al., 1999) and finite mixture components (Galbraith, 2005)) calculated in the R-Lum package (Kreutzer et.al. 2012). The mean equivalent doses are similar to the apparent doses observed in the laboratory profile measurements, and dose distributions in all cases indicate mixed age material as expected.

Table 3.5: Summary of mean, weighted mean and robust mean equivalent doses, and with doses calculated using a Minimum Age Model (MAM) and a Finite Mixture Model (FMM).

Sample	n	Equivalent Dose (Gy)				FMM	FMM
		Mean	Weighted mean	Robust mean	MAM	Component 1	Component 2
3190/8	6	5.9 ± 1.3	6.07 ± 0.47	6.48 ± 0.50	6.42 ± 1.05	6.32 ± 1.18	8.27 ± 0.28
3190/11	36	6.5 ± 0.5	4.29 ± 0.14	6.28 ± 0.15	3.78 ± 0.41	4.15 ± 0.35	7.17 ± 0.39
3190/12	28	6.8 ± 1.1	4.23 ± 0.11	5.37 ± 0.13	3.88 ± 0.39	3.92 ± 0.25	5.37 ± 0.63

The dose distribution for SUTL3190/8 (Fig. 3.1) show the majority of aliquots giving equivalent dose values in the 5-10Gy range, with mean values in the 6.0-6.5Gy range. There is slight evidence of two dose components in the distribution, although this is based on just 6 aliquots and is thus not conclusive.

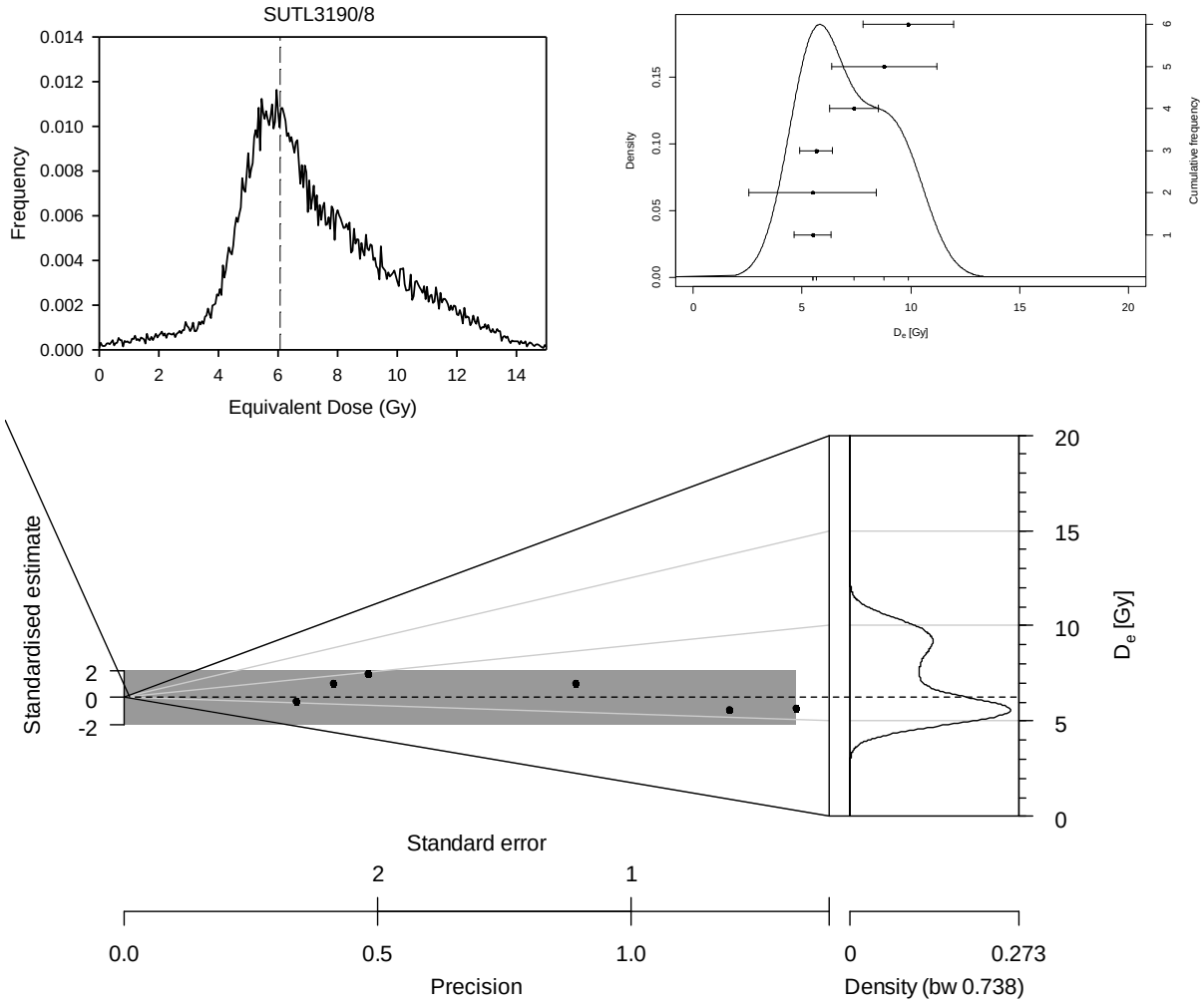

Figure 3.1: Dose distributions for 6 aliquots from SUTL3190/8, displayed as probability density function (top left) kernel density estimation (top right) and abanico plot (bottom). Dashed lies indicate the weighted mean.

The dose distribution for SUTL3190/11 (Fig. 3.2) show three apparent components, one around 2Gy produced from just two aliquots, one at around 4Gy and the third at around 7Gy, with a tail higher doses. The majority of aliquots give low precision equivalent dose values in the 4-8Gy region, giving the mean values at about 6Gy. Of the two aliquots giving the component around 2Gy, one has very low precision, and therefore as this is driven mainly by a single aliquot it is not considered significant (the FMM dose for this has not been included in Table 3.5).

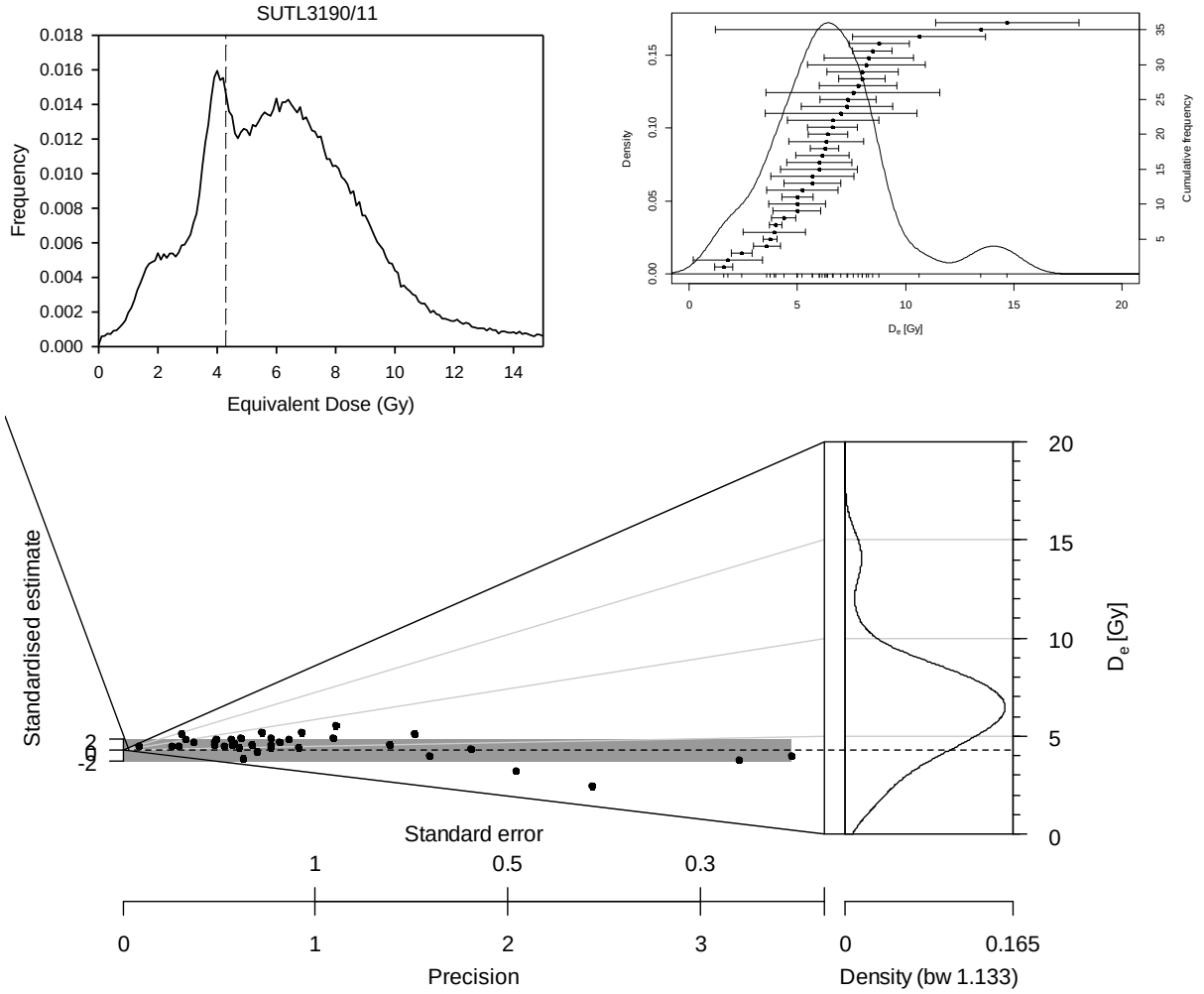

Figure 3.2: Dose distributions for 36 aliquots from SUTL3190/11, displayed as probability density function (top left) kernel density estimation (top right) and abanico plot (bottom). Dashed lies indicate the weighted mean.

The dose distribution for SUTL3190/12 (Fig. 3.3) show a large component with a narrow equivalent dose range of 3-6Gy, giving rise to a peak at around 4Gy reflected in the weighted mean and the MAM and first FMM component. There is also a tail of lower precision higher dose aliquots.

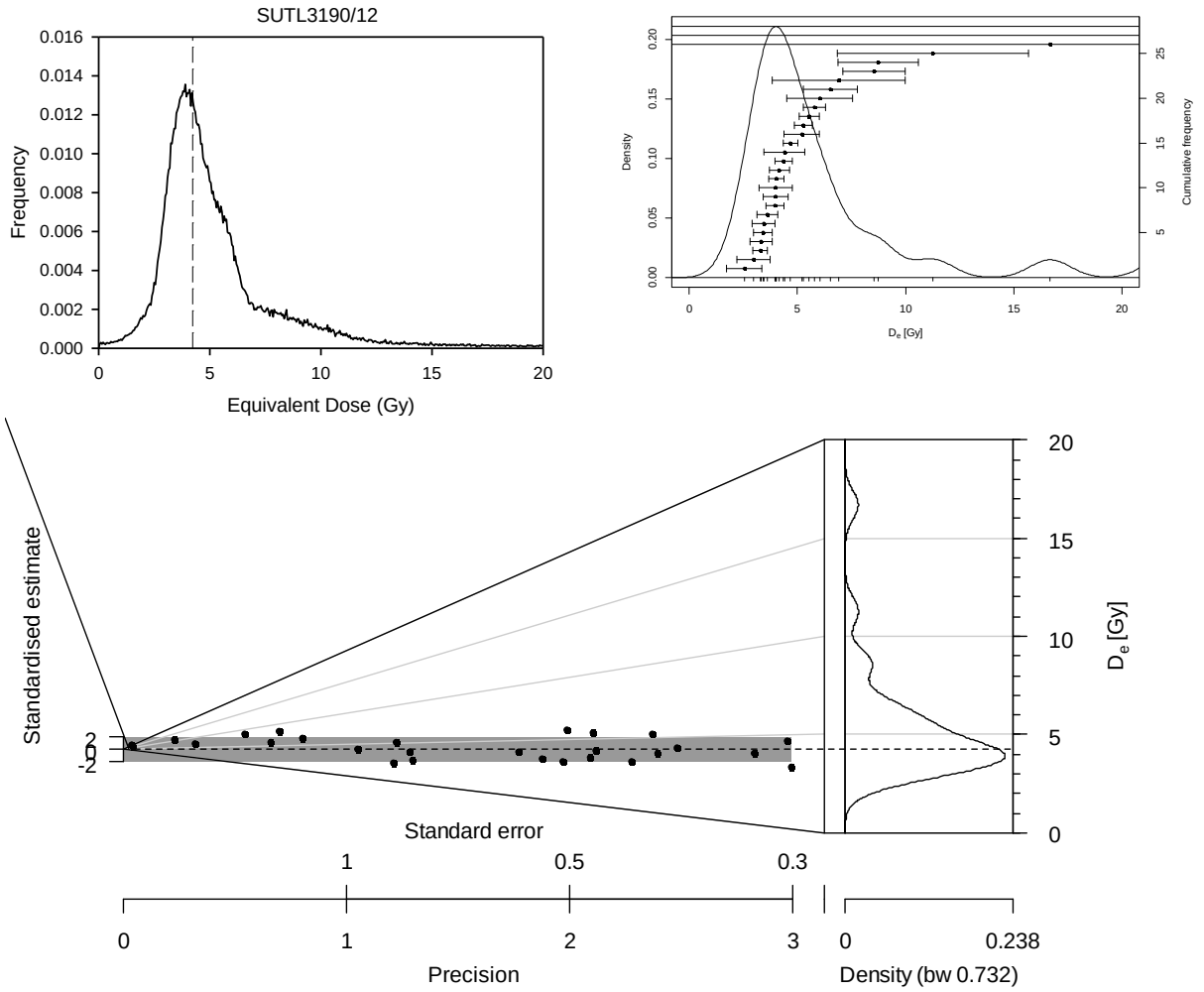

Figure 3.3: Dose distributions for 28 aliquots from SUTL3190/12, displayed as probability density function (top left) kernel density estimation (top right) and abanico plot (bottom). Dashed lies indicate the weighted mean.

The top two samples (SUTL3190/8 and SUTL3190/11) are taken from material given a preliminary association with the bank material. Both contain a majority of aliquots that give low precision equivalent doses with a mean around 6Gy. The lower of these also contains a few higher precision lower equivalent dose values giving a component around 4 Gy. The lower sample (SUTL3190/12) was taken from material preliminarily identified as the old ground surface on which the bank was constructed. This contains a majority of aliquots with equivalent doses forming a tightly defined group with a mean dose of around 4Gy.

3.5. Age Determinations

Ages, and corresponding calendar dates, are determined from the equivalent dose (Table 3.5) and dose rate (Table 3.3), as shown in Table 3.6.

SUTL3190/12 provides the clearest individual sample date. The weighted mean equivalent dose gives a 2.00 ± 0.11ka age (20 ± 120AD), and is a reasonable value for the mean of the low dose components. The MAM and FMM give a slightly lower dose value, which is largely driven by two lower dose aliquots which also have slightly lower precision, giving a slightly younger age of 1.85 ± 0.17ka (180 ± 180AD). Given the lower precision of the youngest aliquots, the date produced from the weighted mean is preferred.

SUTL3190/8 gives a single broad dose distribution, with a weighted mean that gives a 2.56 ± 0.47ka age (530 ± 250 BC).

SUTL3190/11 gives two significant components in the dose distribution, one dominating the higher precision aliquots gives the weighted mean producing a 2.01 ± 0.12ka age (15 ± 120AD), the other component gives an age from the FMM of 3.36 ± 0.25ka (1340 ± 250BC). This appears to represent a mixture of aliquots, some with the same age as SUTL319/12 immediately below it and some with an age slightly older but consistent with the bank material in SUTL3190/8.

Table 3.6: Ages and corresponding calendar dates for each sample, with different equivalent dose components from Table 3.5. Preferred values in bold.

Sample	Dose Rate mGy a^{-1}	Equivalent Dose Gy	Age ka	Date
SUTL3190/8	2.37 ± 0.12	6.07 ± 0.47†	2.56 ± 0.24	530 ± 250 BC
SUTL3190/11	2.13 ± 0.11	**4.29 ± 0.14†**	**2.01 ± 0.12**	**15 ± 120 AD**
		7.17 ± 0.39‡	3.36 ± 0.25	1340 ± 250 BC
SUTL3190/12	2.11 ± 0.11	**4.23 ± 0.11†**	**2.00 ± 0.11**	**20 ± 120 AD**
		3.9 ± 0.3*	1.85 ± 0.17	180 ± 180 AD

† Weighted mean ‡ FMM Component * MAM

4. Discussion and conclusions

Portable OSL measurements showed a high degree of reproducibility between the paired aliquots taken from the monolith, with all but the bottom samples showing similar OSL and IRSL counts and depletion indices. The bottom sample, SUTL3190/12 at 48cm, and to a smaller extent the sample above this, SUTL3190/11 at 44cm, showed smaller OSL and IRSL counts and a higher OSL depletion index. The laboratory profile measurements support this, with no significant variation in sensitivity between samples and a lower apparent dose from OSL for the bottom sample. The TL measurements show three distinct zones within the monolith which approximately correspond to the three main contexts identified in the excavation report, with higher apparent doses (200-1000Gy) in the top 25cm identified as top soil or dark sediment (contexts 1 and 2) interpreted as soils developed on the monument after construction as they extend across the bank and ditch fills, medium apparent doses (50-200Gy) in orange silt (context 5) interpreted as the bank material derived from the ditch, and lower apparent doses (<50Gy) in the bottom sample within the compacted sediment (context 8) interpreted as the natural subsoil exposed at the time of rampart construction in this location.

The luminescence profiles are consistent with the field interpretation. Confirmation from luminescence measurements that the compacted sediment (context 8) is the natural through which the ditch was dug and on which the bank was constructed would, however, require samples below the bottom of the monolith showing increasing signals and apparent ages. In further work on this or similar sites it is recommended that luminescence profile samples are collected from deeper into the apparent natural material to provide additional data to confirm the interpretation of the stratigraphy.

On the basis of these observations and the prior identification of the different contexts within the monolith, three points were selected for OSL dating – SUTL3190/8 (30cm) at the top of the orange silt (context 5) bank material, SUTL3190/11 (44cm) at the bottom of the orange silt, and SUTL3190/12 (48cm) in the compacted orange silt (context 8) interpreted as the natural subsoil exposed at the time of construction. Material was removed from these locations for both dose rate determination and OSL dating, additional material from two other locations was collected for HRGS to determine whether gamma dose rates varied significantly down the section.

On the assumption that SUTL3190/12 is from the old ground surface and contains mineral grains that had had their luminescence signals removed by exposure to daylight before burial under the bank, the 20 ± 120AD date for this sample provides a terminus post quem (TPQ) for the construction of this section of the bank. The sample immediately above this, SUTL3190/11, contains a mixture of two age components, one of which is identical to the apparent old ground surface at 15 ± 120AD, and the other is older and lower precision at 1340 ± 250BC. Assuming the younger of these dates corresponds to the same bleaching event as the SUTL3190/12 sample, either being a mixture of old surface and bank or incorporating the old surface material excavated from the ditch, the combination of these two dates gives a date for this event of 20 ± 85AD. This date is consistent with construction of the earthworks at this location in the late Iron Age or early Roman period and is inconsistent with suggestions that this part of the enclosure is associated with the medieval motte and also does not support the possibility of there having been a preceding Neolithic enclosure.

The two samples from the supposed bank material also contain minerals with older ages, as would be expected from material excavated from the ditch which experienced limited exposure to daylight.

5. References

Aitken, M.J., 1983, Dose rate data in SI units: PACT, v. 9, p. 69–76.

AMC 2001, Robust statistics: a method of coping with outliers. *amc technical brief.* Analytical Methods Committee, The Royal Society of Chemistry. https://www.rsc.org/images/robust-statistics-technical-brief-6_tcm18-214850.pdf

Bøtter-Jensen, L., Bulur, E., Duller, G.A.T., and Murray, A.S., 2000, Advances in luminescence instrument systems: *Radiation Measurements*, v. 32, p. 523-528.

Cresswell, A.J., Carter, J., Sanderson, D.C.W., 2018, Dose rate conversion parameters: assessment of nuclear data. *Radiation Measurements* 120, 195-201. doi 10.1016/j.radmeas.2018.02.007

Dietze, M., Kreutzer, S., Fuchs, M.C., Burow, C., Fischer, M., Schmidt, C., 2013. A practical guide to the R package Luminescence. *Ancient TL*, 31, pp. 11-18.

Galbraith, R.F., Roberts, R.G., Laslett, G.M., Yoshida, H. & Olley, J.M., 1999. Optical dating of single grains of quartz from Jinmium rock shelter, northern Australia. Part I: experimental design and statistical models. *Archaeometry*, 41, pp. 339-364.

Galbraith, R.F., 2005. *Statistics for Fission Track Analysis*, Chapman & Hall/CRC, Boca Raton

Hankinson, R., 2022. *Twmbarlwm: Archaeological Investigation*, Unpublished CPAT Report No 1820.

Kreutzer, S., Schmidt, C., Fuchs, M.C., Dietze, M., Fischer, M., Fuchs, M., 2012. Introducing an R package for luminescence dating analysis. *Ancient TL*, 30, pp. 1-8.

Mejdahl, V., 1979, Thermoluminescence dating: Beta-dose attenuation in quartz grains Archaeometry, v. 21, p. 61-72.

Mejdahl, V., 1983, Feldspar inclusion dating of ceramics and burnt stones, PACT, v. 9, p. 351-364.

Murray, A.S., and Wintle, A.G., 2000, Luminescence dating of quartz using an improved single-aliquot regenerative-dose protocol: *Radiation Measurements*, v. 32, p. 57-73.

NEA, 2000, The JEF-2.2 Nuclear Data Library: Nuclear Energy Agency, Organisation for economic Co-operation and Development. JEFF Report, v. 17.

Prescott, J.R., and Hutton, J.T., 1994, Cosmic ray contributions to dose rates for luminescence and ESR dating: Large depths and long-term time variations: *Radiation Measurements*, v. 23, p. 497-500.

Sanderson, D.C.W., 1987, Thermoluminescence dating of vitrified Scottish Forts: Paisley, Paisley college.

—, 1988, Thick source beta counting (TSBC): A rapid method for measuring beta dose-rates: International Journal of Radiation Applications and Instrumentation. Part D. Nuclear Tracks and Radiation Measurements, v. 14, p. 203-207.

Sanderson, D.C.W., and Murphy, S., 2010, Using simple portable OSL measurements and laboratory characterisation to help understand complex and heterogeneous sediment sequences for luminescence dating: Quaternary Geochronology, v. 5, p. 299-305.

Appendix A: Portable OSL Data

Table A.1: Portable OSL data for SUTL3190

Sample	IRSL		OSL		IRSL : OSL
	Net counts	Depletion	Net counts	Depletion	
SUTL3190/1A	5578 ± 85	1.32 ± 0.04	48737 ± 225	1.38 ± 0.01	0.114 ± 0.002
SUTL3190/1B	7878 ± 98	1.29 ± 0.03	58462 ± 245	1.37 ± 0.01	0.135 ± 0.002
SUTL3190/2A	5685 ± 86	1.31 ± 0.04	60118 ± 249	1.39 ± 0.01	0.095 ± 0.001
SUTL3190/2B	9717 ± 107	1.34 ± 0.03	80375 ± 288	1.35 ± 0.01	0.121 ± 0.001
SUTL3190/3A	8433 ± 100	1.21 ± 0.03	64300 ± 258	1.37 ± 0.01	0.131 ± 0.002
SUTL3190/3B	7391 ± 97	1.33 ± 0.04	55492 ± 240	1.37 ± 0.01	0.133 ± 0.002
SUTL3190/4A	8409 ± 102	1.34 ± 0.03	66342 ± 262	1.36 ± 0.01	0.127 ± 0.002
SUTL3190/4B	5769 ± 86	1.24 ± 0.04	57423 ± 244	1.32 ± 0.01	0.100 ± 0.002
SUTL3190/5A	9652 ± 106	1.31 ± 0.03	68405 ± 266	1.42 ± 0.01	0.141 ± 0.002
SUTL3190/5B	8455 ± 100	1.26 ± 0.03	66631 ± 262	1.34 ± 0.01	0.127 ± 0.002
SUTL3190/6A	5890 ± 88	1.30 ± 0.04	49177 ± 226	1.38 ± 0.01	0.120 ± 0.002
SUTL3190/6B	6508 ± 89	1.35 ± 0.04	62737 ± 254	1.39 ± 0.01	0.104 ± 0.001
SUTL3190/7A	10609 ± 110	1.30 ± 0.03	80291 ± 287	1.43 ± 0.01	0.132 ± 0.001
SUTL3190/7B	4621 ± 79	1.35 ± 0.05	53321 ± 235	1.29 ± 0.01	0.087 ± 0.002
SUTL3190/8A	8796 ± 103	1.33 ± 0.03	85430 ± 296	1.34 ± 0.01	0.103 ± 0.001
SUTL3190/8B	6335 ± 89	1.30 ± 0.04	63134 ± 255	1.40 ± 0.01	0.100 ± 0.001
SUTL3190/9A	6395 ± 89	1.26 ± 0.04	62989 ± 255	1.40 ± 0.01	0.102 ± 0.001
SUTL3190/9B	7151 ± 93	1.31 ± 0.03	63240 ± 256	1.38 ± 0.01	0.113 ± 0.002
SUTL3190/10A	7315 ± 95	1.29 ± 0.03	63312 ± 256	1.47 ± 0.01	0.116 ± 0.002
SUTL3190/10B	5394 ± 85	1.30 ± 0.04	52486 ± 233	1.39 ± 0.01	0.103 ± 0.002
SUTL3190/11A	6017 ± 88	1.36 ± 0.04	42129 ± 210	1.51 ± 0.02	0.143 ± 0.002
SUTL3190/11B	3788 ± 71	1.31 ± 0.05	41518 ± 208	1.48 ± 0.02	0.091 ± 0.002
SUTL3190/12A	869 ± 53	1.49 ± 0.19	25975 ± 167	1.99 ± 0.03	0.033 ± 0.002
SUTL3190/12B	2193 ± 63	1.30 ± 0.08	31689 ± 183	1.90 ± 0.02	0.069 ± 0.002

Appendix B: Laboratory Profiling Data

Table B.1: Sensitivity, sensitivity change (ratio of final to initial test dose responses) and apparent dose for the OSL measurements of nominal quartz from SUTL3190.

Sample	Sensitivity (c/Gy)			Sensitivity change			Apparent Dose (Gy)		
	Al 1	Al 2	Mean	Al 1	Al 2	Mean	Al 1	Al 2	Mean
SUTL3190/1	50 ± 34	-14 ± 36	18 ± 25	0.22 ± 0.75	-7.5 ± 18.8	-3.62 ± 9.4	5.5 ± 1.6	-0.5 ± 1.6	2.5 ± 1.1
SUTL3190/2	43 ± 58	9 ± 37	26 ± 34	-2.03 ± 3.07	-4.5 ± 19.2	-3.26 ± 9.71	1.3 ± 0.8	-4.0 ± 7.4	-1.4 ± 3.7
SUTL3190/3	213 ± 50	-47 ± 35	83 ± 30	0.40 ± 0.22	-1.02 ± 1.06	-0.31 ± 0.54	27.3 ± 3.1	1.2 ± 3.5	14.3 ± 2.4
SUTL3190/4	14 ± 32	-67 ± 36	-26 ± 24	-5.2 ± 11.9	0.20 ± 0.55	-2.52 ± 5.93	-41.5 ± 66.2	-64 ± 218	-52.8 ± 113.9
SUTL3190/5	140 ± 42	52 ± 39	96 ± 28	0.65 ± 0.35	2.94 ± 2.31	1.79 ± 1.17	11.5 ± 2.6	6.7 ± 1.7	9.1 ± 1.6
SUTL3190/6	30 ± 39	4366 ± 91	2198 ± 50	4.22 ± 5.72	0.76 ± 0.03	2.49 ± 2.86	15.7 ± 7.2	28.9 ± 0.4	22.3 ± 3.6
SUTL3190/7	177 ± 38	313 ± 43	245 ± 29	1.71 ± 0.44	1.18 ± 0.22	1.44 ± 0.25	3.8 ± 0.4	4.2 ± 0.3	4.0 ± 0.2
SUTL3190/8	111 ± 36	140 ± 39	126 ± 27	-1.17 ± 0.53	0.57 ± 0.33	-0.30 ± 0.31	6.4 ± 2.1	4.8 ± 0.6	5.6 ± 1.1
SUTL3190/9	430 ± 67	43 ± 40	236 ± 39	0.39 ± 0.15	2.23 ± 2.26	1.31 ± 1.13	40.7 ± 3.0	6.6 ± 1.9	23.7 ± 1.8
SUTL3190/10	62 ± 44	554 ± 91	308 ± 50	-1.32 ± 1.21	0.60 ± 0.19	-0.36 ± 0.61	6.0 ± 3.2	5.2 ± 0.4	5.6 ± 1.6
SUTL3190/11	239 ± 44	130 ± 43	185 ± 30	1.55 ± 0.35	0.82 ± 0.44	1.19 ± 0.28	4.4 ± 0.3	6.7 ± 1.6	5.6 ± 0.8
SUTL3190/12	83 ± 39	197 ± 39	140 ± 27	0.24 ± 0.53	2.78 ± 0.59	1.51 ± 0.39	2.4 ± 1.1	3.6 ± 0.2	3.0 ± 0.6

Table B.2: Sensitivity, sensitivity change (ratio of final to initial test dose responses) and apparent dose for the OSL measurements of polymineral from SUTL3190.

Sample	Sensitivity (c/Gy)			Sensitivity change			Apparent Dose (Gy)		
	Al 1	Al 2	Mean	Al 1	Al 2	Mean	Al 1	Al 2	Mean
SUTL3190/1	6 ± 5	19 ± 6	12 ± 4	2.96 ± 3.06	1.31 ± 0.52	2.14 ± 1.55	494 ± 481	11.3 ± 4.2	253 ± 241
SUTL3190/2	28 ± 6	21 ± 6	25 ± 4	1.20 ± 0.34	0.94 ± 0.38	1.07 ± 0.26	16.3 ± 3.8	35.1 ± 9.8	25.7 ± 5.2
SUTL3190/3	38 ± 6	0 ± 6	19 ± 4	0.99 ± 0.24	35.5 ± 487.0	18.3 ± 243.5	15.3 ± 2.9	1834 ± 25152	925 ± 12576
SUTL3190/4	7 ± 6	12 ± 6	10 ± 4	4.76 ± 4.08	-0.75 ± 0.63	2.01 ± 2.06	29 ± 24.7	22.8 ± 12.1	25.9 ± 13.8
SUTL3190/5	18 ± 6	197 ± 9	107 ± 5	0.52 ± 0.39	1.47 ± 0.08	0.99 ± 0.20	25.4 ± 8.9	13.1 ± 0.7	19.3 ± 4.5
SUTL3190/6	26 ± 6	13 ± 6	19 ± 4	2.06 ± 0.51	2.07 ± 1.16	2.06 ± 0.64	11.4 ± 3.0	71.5 ± 36.4	41.5 ± 18.3
SUTL3190/7	52 ± 6	29 ± 6	40 ± 4	0.60 ± 0.15	0.73 ± 0.25	0.66 ± 0.15	8.9 ± 1.4	24.0 ± 5.4	16.4 ± 2.8
SUTL3190/8	42 ± 6	163 ± 8	103 ± 5	1.18 ± 0.24	1.77 ± 0.11	1.47 ± 0.13	11.6 ± 2.0	9.8 ± 0.6	10.7 ± 1.0
SUTL3190/9	27 ± 6	28 ± 6	28 ± 4	1.79 ± 0.5	0.88 ± 0.29	1.34 ± 0.29	23.5 ± 5.9	10.4 ± 2.5	16.9 ± 3.2
SUTL3190/10	35 ± 6	24 ± 6	30 ± 4	0.94 ± 0.25	1.04 ± 0.38	0.99 ± 0.23	16.5 ± 3.2	17.6 ± 4.8	17.0 ± 2.9
SUTL3190/11	10 ± 6	193 ± 8	101 ± 5	1.44 ± 1.05	1.88 ± 0.10	1.66 ± 0.52	79.2 ± 46.7	11.2 ± 0.6	45.2 ± 23.3
SUTL3190/12	73 ± 8	99 ± 8	86 ± 5	2.11 ± 0.24	1.85 ± 0.17	1.98 ± 0.15	13.9 ± 1.6	10.8 ± 1.0	12.3 ± 0.9

Table B.3: Sensitivity, sensitivity change (ratio of final to initial test dose responses) and apparent dose for the IRSL measurements of polymineral grains from SUTL3190.

Sample	Sensitivity (c/Gy)			Sensitivity change			Apparent Dose (Gy)		
	Al 1	Al 2	Mean	Al 1	Al 2	Mean	Al 1	Al 2	Mean
SUTL3190/1	6 ± 5	-10 ± 5	-2 ± 4	2.47 ± 2.13	-0.86 ± 0.66	0.80 ± 1.11	2791 ± 2249	-204 ± 102	1293 ± 1125
SUTL3190/2	4 ± 5	8 ± 5	6 ± 3	2.11 ± 2.87	0.61 ± 0.65	1.36 ± 1.47	178.5 ± 219.2	684 ± 383	431 ± 221
SUTL3190/3	9 ± 5	12 ± 5	10 ± 3	2.16 ± 1.29	0.91 ± 0.58	1.53 ± 0.71	272.0 ± 148.3	545 ± 229	411 ± 136
SUTL3190/4	-1 ± 5	12 ± 5	5 ± 3	1.00 ± 4.94	0.23 ± 0.40	0.62 ± 2.48	-665 ± 2321	32.9 ± 12.3	-316 ± 1160
SUTL3190/5	30 ± 5	-1 ± 5	15 ± 4	0.91 ± 0.23	16.5 ± 102.2	8.7 ± 51.1	48.4 ± 8.3	-3853 ± 23830	-1902 ± 11915
SUTL3190/6	12 ± 5	14 ± 5	13 ± 3	0.88 ± 0.57	1.29 ± 0.58	1.08 ± 0.41	137 ± 55	332 ± 111	234.2 ± 62.1
SUTL3190/7	24 ± 5	31 ± 5	28 ± 3	-0.16 ± 0.19	0.76 ± 0.20	0.30 ± 0.14	99.2 ± 19.1	16.9 ± 3.1	58.0 ± 9.7
SUTL3190/8	5 ± 5	-4 ± 5	0 ± 3	2.42 ± 2.63	-0.81 ± 1.28	0.80 ± 1.46	42.7 ± 43.2	-32.6 ± 34.5	5.0 ± 27.6
SUTL3190/9	18 ± 6	-12 ± 4	3 ± 4	1.94 ± 0.69	-0.88 ± 0.48	0.53 ± 0.42	39.1 ± 12.5	-108.3 ± 40.7	-34.6 ± 21.3
SUTL3190/10	21 ± 5	8 ± 5	15 ± 4	0.29 ± 0.26	-0.46 ± 0.71	-0.09 ± 0.38	41.5 ± 10.6	55.1 ± 33.8	48.3 ± 17.7
SUTL3190/11	30 ± 5	9 ± 5	20 ± 4	0.49 ± 0.19	3.09 ± 1.80	1.79 ± 0.91	362 ± 64	904 ± 498	633 ± 251
SUTL3190/12	-5 ± 5	0 ± 5	-2 ± 4	-0.20 ± 1.06	5.0 ± 120.5	2.4 ± 60.2	-21.9 ± 22.2	1364 ± 32183	671 ± 16092

Table B.4: Sensitivity, sensitivity change (ratio of final to initial test dose responses) and apparent dose for the TL measurements of polymineral grains from SUTL3190.

Sample	Sensitivity (c/Gy)			Sensitivity change			Apparent Dose (Gy)		
	Al 1	Al 2	Mean	Al 1	Al 2	Mean	Al 1	Al 2	Mean
SUTL3190/1	82 ± 4	102 ± 5	92 ± 3	1.173 ± 0.080	0.822 ± 0.055	0.998 ± 0.049	1011 ± 51	363.6 ± 16.5	687.5 ± 26.7
SUTL3190/2	132 ± 5	52 ± 3	92 ± 3	1.033 ± 0.057	-0.270 ± 0.043	0.381 ± 0.036	281.3 ± 11.2	571.3 ± 36.1	426.3 ± 18.9
SUTL3190/3	90 ± 4	188 ± 6	139 ± 4	0.806 ± 0.058	0.486 ± 0.028	0.646 ± 0.032	299.9 ± 14.4	207.7 ± 7.0	253.8 ± 8.0
SUTL3190/4	61 ± 4	42 ± 3	52 ± 2	0.913 ± 0.077	1.510 ± 0.137	1.211 ± 0.078	275.9 ± 16.1	362.4 ± 25.7	319.1 ± 15.2
SUTL3190/5	182 ± 6	252 ± 7	217 ± 5	0.592 ± 0.033	0.662 ± 0.030	0.627 ± 0.022	127.5 ± 4.4	203.8 ± 5.9	165.7 ± 3.7
SUTL3190/6	39 ± 3	50 ± 3	44 ± 2	0.968 ± 0.101	1.103 ± 0.098	1.035 ± 0.070	339.2 ± 25	714.5 ± 46	526.8 ± 26.2
SUTL3190/7	113 ± 5	81 ± 4	97 ± 3	1.351 ± 0.076	1.310 ± 0.088	1.331 ± 0.058	268 ± 11.5	355.9 ± 18.1	312.0 ± 10.7
SUTL3190/8	109 ± 5	131 ± 5	120 ± 4	1.253 ± 0.073	0.399 ± 0.030	0.826 ± 0.039	68.3 ± 3.1	73.5 ± 3.0	70.9 ± 2.2
SUTL3190/9	93 ± 4	62 ± 4	77 ± 3	2.236 ± 0.127	1.454 ± 0.109	1.845 ± 0.083	82.5 ± 4.0	123.4 ± 7.2	102.9 ± 4.1
SUTL3190/10	172 ± 6	55 ± 3	114 ± 3	1.072 ± 0.052	0.981 ± 0.085	1.027 ± 0.050	105.6 ± 3.7	141.8 ± 8.8	123.7 ± 4.8
SUTL3190/11	157 ± 6	225 ± 7	191 ± 4	0.933 ± 0.049	1.193 ± 0.049	1.063 ± 0.034	149.1 ± 5.5	195.3 ± 6.0	172.2 ± 4.1
SUTL3190/12	202 ± 6	233 ± 7	217 ± 5	0.836 ± 0.040	0.391 ± 0.022	0.613 ± 0.023	30.9 ± 1.1	33.4 ± 1.1	32.2 ± 0.8

Appendix C: Dose Response Curves

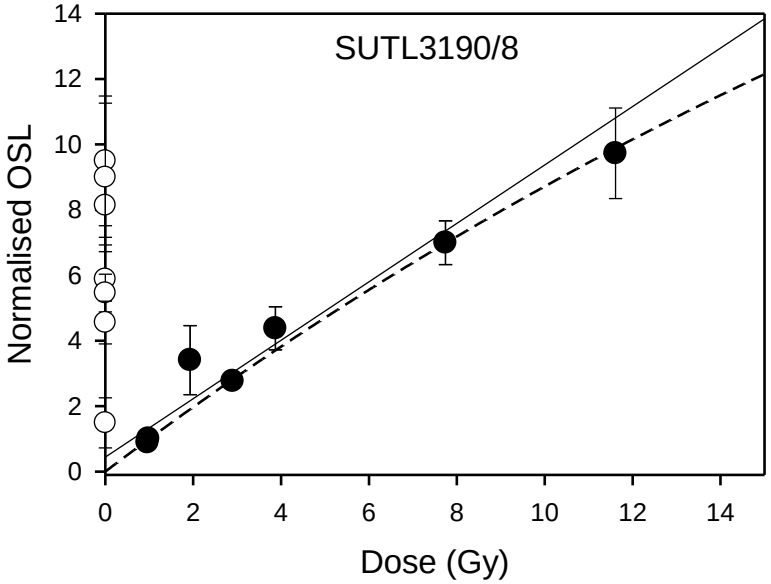

Figure C.1: Dose response curve for SUTL3190/8, showing linear regression (solid line) through 0-8Gy data, saturating exponential curve (dashed line) through all data, and normalised natural signals (open circles on y-axis).

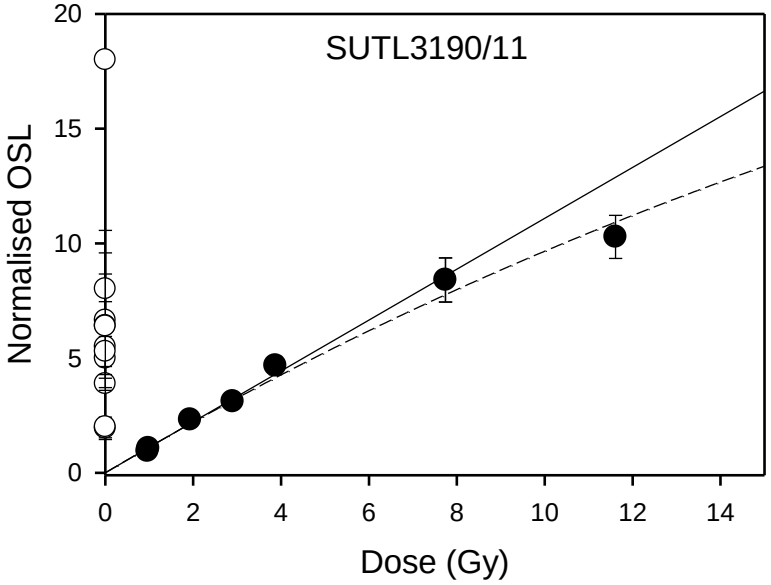

Figure C.2: Dose response curve for SUTL3190/11, showing linear regression (solid line) through 0-8Gy data, saturating exponential curve (dashed line) through all data, and normalised natural signals (open circles on y-axis).

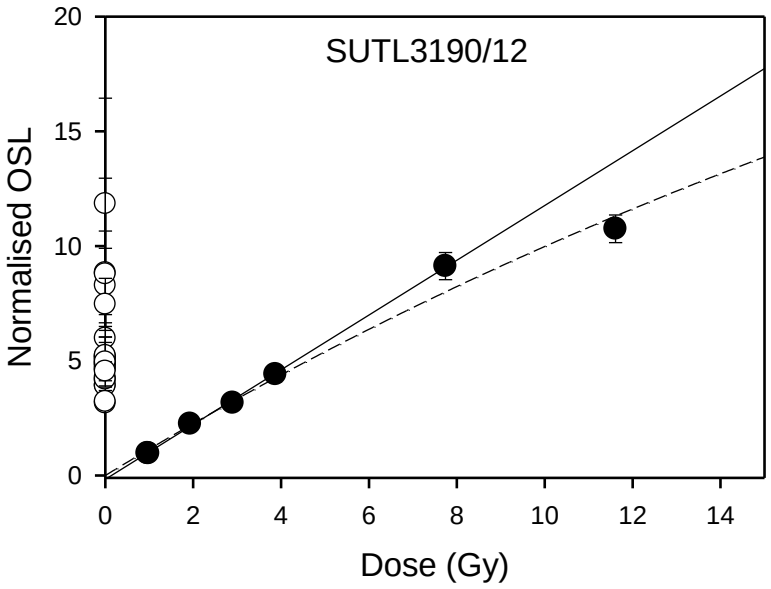

Figure C.3: Dose response curve for SUTL3190/12, showing linear regression (solid line) through 0-8Gy data, saturating exponential curve (dashed line) through all data, and normalised natural signals (open circles on y-axis).